Appl. Phys. B 65, 713–724 (1997)

Applied Physics B Lasers and Optics

Multiple beam atom interferometer: theory and experiment

M. Weitz, T. Heupel, T.W. Hänsch

Max-Planck-Institut für Quantenoptik, 85748 Garching, Germany

Received: 30 May 1997/ 27 August 1997

Abstract. We first give a detailed account of the theory of atom interferometers based on a sequence of laser pulses projecting the atomic wave packets onto a spatially separating dark superposition state. We then describe the experimental realization of a multiple beam atom interferometer based on this method. In our experiment, we observe an interference signal that shows the sharply peaked Airy-function like pattern characteristic for multiple beam interference. Besides this fringe sharpening effect, we observe a further significant difference compared to the signal of a conventional two-beam atom interferometer. When the time between the beamsplitting pulses is varied, we observe collapse and revival of the fringe pattern, which is caused by a recoil phase shift increasing quadratically with the transverse atomic momentum.

PACS: 03.75.Dg; 07.60.Ly; 42.50.Vk; 32.80.Lg

In recent years, we have witnessed much progress in two-beam interferometry with neutral atoms [1]. Compared to the field of interferometry with electrons [2] and neutrons [3], the additional internal structure of atoms allows their efficient manipulation with resonant laser light. Moreover, quantum mechanical superpositions with entangled internal and external states, such as velocity dependent dark states can be realized, which introduces novel possibilities for the manipulation of matter waves.

In this work, we give a theory of atom interferometers using velocity dependent dark states, and describe the experimental realization of a multiple beam atom interferometer based on this method. The interferometer has been realized with a sequence of three laser pulses projecting the atomic wave packets onto such velocity dependent dark states. Whereas in all previous atom interferometer experiments sinusoidal signals resulting from two-beam interference have been observed, the interference signal of our experiment resembles the Airy function known from optical multiple beam interference [4], such as e.g. a Fabry-Pérot interferometer. The peaks are sharper than the sinusoidal fringes observed in a two-beam atom interferometer, which translates into a higher resolution. We have also observed some further effects intimately connected to multiple beam interference in the presence of a phase increasing quadratically with transverse atomic momentum. When the drift time between the beam splitting pulses is varied, we observe collapse and revival of the fringe pattern.

In our experiment an atom is coherently split into more than two atomic wave packets by optical pumping into a dark velocity dependent multilevel superposition state. The momenta of two adjacent paths differ by two photon momenta. We use a cesium atomic beam and two counterpropagating optical beams in a $\sigma^+ - \sigma^-$ polarization configuration tuned to the $6S_{1/2}\,(F=4) - 6P_{1/2}\,(F'=4)$ transition of the cesium D1-line. In a first laser pulse, cesium atoms are optically pumped into a dark superposition of the five even magnetic ground state sublevels ($m_F = -4, -2, \ldots, 4$). The momenta of the atoms in these sublevels are $0, 2\hbar\boldsymbol{k}, \ldots, 8\hbar\boldsymbol{k}$ relative to the momentum of the $m_F = -4$ sublevel (Fig. 1). The paths spatially separate for a time T, after which a second laser pulse is applied. By this time, provided that the splitting between the paths exceeds the atomic coherence length, the atom can no longer be completely dark for the light field. In a different basis, each path can be decomposed into a dark state and several coupled state components. The second pulse projects again onto a dark state by optically pumping all other components into the $F = 3$ hyperfine ground state, which is not detected. In this way, the second pulse splits each of the five paths further into five. At time T after the second pulse several paths cross. A third optical pulse now closes the interferometer, and the wave packets in the recombined paths interfere.

Quantum mechanical coherent superpositions with entangled external and internal states have been used in subrecoil laser cooling with the aim of accumulating atoms in a dark state ("velocity selective coherent population trapping") [5]. Marte, Zoller and Hall suggested to coherently split up an atomic wave packet by adiabatic passage through a velocity dependent dark state [6], which was followed by demonstrations of momentum transfer with adiabatic passage [7, 8]. Shortly afterwards, an atomic two-beam interferometer based on a dark state in a three-level system was demonstrated [9]. In that work the "dark state" analogon of an optical Ramsey

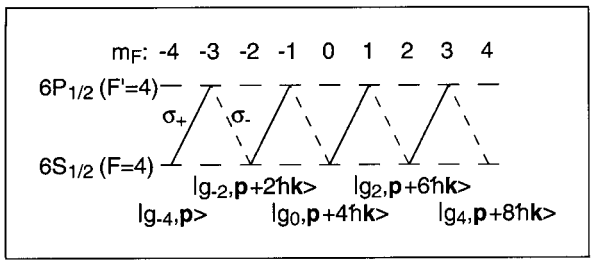

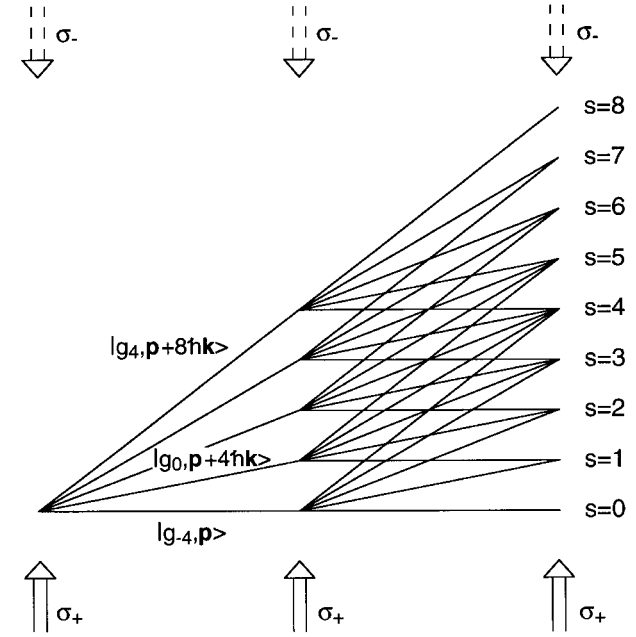

Fig. 1. The inset shows the level scheme for a velocity dependent dark state using the $6S_{1/2}\,(F=4)-6P_{1/2}\,(F'=4)$ transition of the cesium D1 line, and two conterpropagating optical beams in a $\sigma^+-\sigma^-$ polarization configuration. The dark state here is a coherent superposition of the five even magnetic ground state sublevels with the momenta of adjacent components differing by two photon recoils. *Bottom*: Scheme of an atomic multiple beam interferometer realized with a sequence of three laser pulses. The atoms interfere in different families of wave packets numbered: $s = 0, 1, \ldots, 8$

experiment (or $4\pi/2$ pulse interferometer [10]) was realized. Here we use a "dark state" analogon of the $\pi/2$–π–$\pi/2$ pulse interferometer [11] with a pulse sequence of NMR spin echo experiments [12]. Whereas a superposition of spatially separating wave packets previously was generated by adiabatic passage, we here are coherently splitting up a path by simply projecting the atomic wave packets onto a spatially separating dark superposition state. Note that in contrast to the work on laser cooling [5], where atoms are accumulated in a dark state through the use of a closed transition, in our case it is essential to use an open optical transition at least for the second and third laser pulse in order to avoid a large background to the fringe pattern. Our method is applicable both to three- and multilevel systems, resulting in two- respectively multiple beam interference.

Recently we have reported on the first realization of a multiple beam interferometer [13]. Later, longer drift times between the atomic beamsplitters have been obtained, which allow the observation of collapse and revival of the fringe pattern [14]. The purpose of the present paper is mainly to give a detailed account of the calculation of the fringe pattern of the interferometer. The theory of interferometers based on projection onto dark states has previously only been briefly sketched. We also review the experimental results obtained.

1 Theory

1.1 Dark states and atomic beamsplitters

We begin this section by considering an atom with a transition from a ground state of total angular momentum F to an excited state with total angular momentum F', which is irradiated with a pair of laser beams of σ^+ respectively σ^- circular polarization. We assume that $F' = F$, since then a single dark state exists. The light couples levels in one family of states forming a chain of V-type transitions where no dark state exists, and a second family of states forming a chain of Λ-type transitions, where one dark state exists. We consider here only the latter family of states. As shown in Fig. 1, the dark state has $N = F+1$ components with only even (or only odd) magnetic quantum numbers. We describe a multiple beam atom interferometer with N paths using such a transition.

The electric field of the two optical beams is assumed to be

$$\boldsymbol{E} = \boldsymbol{E}_{0,+}\cos(\boldsymbol{k}_+\cdot\boldsymbol{r}-\omega_+ t) + \boldsymbol{E}_{0,-}\cos(\boldsymbol{k}_-\cdot\boldsymbol{r}-\omega_- t)\,, \quad (1)$$

where the subscripts + and - refer to the σ^+ respectively σ^- polarized beams. When including the momentum transferred to the atoms by the laser light, one finds that – in the absence of spontaneous emission – families of m_F sublevels with distinct relative momenta must be considered. Transitions are induced only between the following closed family of $2N-1$ (equal to $2F+1$) levels with entangled internal and external states: $|g_{-N+1}, \boldsymbol{p}\rangle$, $|e_{-N+2}, \boldsymbol{p}+\hbar\boldsymbol{k}_+\rangle$, $|g_{-N+3}, \boldsymbol{p}+\hbar(\boldsymbol{k}_+-\boldsymbol{k}_-)\rangle$, $\ldots$, $|g_{N-1}, \boldsymbol{p}+N\hbar(\boldsymbol{k}_+-\boldsymbol{k}_-)\rangle$, where $|g_{m_F}, \boldsymbol{p}\rangle$ and $|e_{m_F}, \boldsymbol{p}\rangle$ denote ground respectively excited states of magnetic quantum number m_F and momentum $\boldsymbol{p}$. In an interaction picture, where the Eigenenergies of the levels are factored out (see e.g. [15]), the Hamiltonian for this basis of levels is

$$\begin{aligned} H = -\frac{\hbar}{2}\sum_{n=1}^{N-1} \Big(& \Omega_+ C_{2n-N-1}^{2n-N}\, \mathrm{e}^{\mathrm{i}t(\Delta_n+\delta_{n-1})} \\ & \times |e_{2n-N}, \boldsymbol{p}+n\hbar\boldsymbol{k}_+-(n-1)\hbar\boldsymbol{k}_-\rangle \\ & \times \langle g_{2n-N-1}, \boldsymbol{p}+(n-1)\hbar(\boldsymbol{k}_+-\boldsymbol{k}_-)| \\ & + \Omega_- C_{2n-N+1}^{2n-N}\, \mathrm{e}^{\mathrm{i}t(\Delta_n+\delta_n)} \\ & \times |e_{2n-N}, \boldsymbol{p}+n\hbar\boldsymbol{k}_+-(n-1)\hbar\boldsymbol{k}_-\rangle \\ & \times \langle g_{2n-N+1}, \boldsymbol{p}+n\hbar(\boldsymbol{k}_+-\boldsymbol{k}_-)| \Big) \\ & + \text{h. c.} \\ & - \frac{\mathrm{i}\hbar\Gamma}{2}\sum_{n=1}^{N-1} |e_{2n-N}, \boldsymbol{p}+n\hbar\boldsymbol{k}_+-(n-1)\hbar\boldsymbol{k}_-\rangle \\ & \times \langle e_{2n-N}, \boldsymbol{p}+n\hbar\boldsymbol{k}_+-(n-1)\hbar\boldsymbol{k}_-|\,, \end{aligned} \quad (2)$$

where

$$\Omega_+ C_{m_F}^{m_F+1} = \frac{e}{\hbar}\left\langle e_{m_F+1}\right| \boldsymbol{r}\cdot\boldsymbol{E}_{0,+}\left|g_{m_F}\right\rangle ,$$
$$\Omega_- C_{m_F}^{m_F-1} = \frac{e}{\hbar}\left\langle e_{m_F-1}\right| \boldsymbol{r}\cdot\boldsymbol{E}_{0,-}\left|g_{m_F}\right\rangle , \quad (3)$$

with $C_{m_F}^{m_{F'}}$ as the Clebsch–Gordan coefficients of the transition from the ground state $|g_{m_F}\rangle$ to the excited state $|e_{m_{F'}}\rangle$. The factors Ω_+, Ω_- denote the Rabi frequencies of the σ^+ and σ^- polarized waves respectively for a transition with a Clebsch–Gordan coefficient of unity. We have accounted for the spontaneous decay of the excited states similarly to [6] by including non-Hermitian terms $-\mathrm{i}\hbar\Gamma/2$ into the Hamiltonian. Further, with ω_{g,m_F} and ω_{e,m_F} as the atomic energies of a ground respectively excited state with magnetic quantum number m_F, the detuning factors (Fig. 2) are given by

$$\begin{aligned}\Delta_n =& -n\omega_+ + (n-1)\omega_- - \omega_{\mathrm{g},-N+1} + \omega_{\mathrm{e},2n-N}\\ &+ \frac{1}{2m\hbar}\left((\boldsymbol{p}+n\hbar\boldsymbol{k}_+ - (n-1)\hbar\boldsymbol{k}_-)^2 - \boldsymbol{p}^2\right), \end{aligned} \quad (4)$$

$$\begin{aligned}\delta_n =& \, n(\omega_+ - \omega_-) + \omega_{\mathrm{g},-N+1} - \omega_{\mathrm{g},2n-N+1}\\ &+ \frac{1}{2m\hbar}\left(\boldsymbol{p}^2 - (\boldsymbol{p}+n\hbar(\boldsymbol{k}_+ - \boldsymbol{k}_-))^2\right),\\ =& \, n\left(\Delta\omega - \frac{(\boldsymbol{k}_+ - \boldsymbol{k}_-)\boldsymbol{p}}{m}\right) - n^2\omega_{\mathrm{r}} . \end{aligned} \quad (5)$$

Since the two-photon detuning δ_n appears in numerous further formulas, the corresponding expression has been simplified by using $\Delta\omega = (\omega_+ - \omega_- - \omega_{\mathrm{Z}})$, with ω_{Z} as the (Zeeman) splitting between two adjacent even (or odd) ground state $\mathrm{m_F}$ levels. Further, $\omega_{\mathrm{r}} = \hbar(\boldsymbol{k}_+ - \boldsymbol{k}_-)^2/2m$ denotes the recoil frequency of a single Raman transition.

When solving for the Eigenvectors of the Hamiltonian (2), one finds one dark state with Eigenvalue zero [16]. The wave function of that state is

$$|\varphi_{\mathrm{D}}(\boldsymbol{p},t)\rangle = \sum_{n=0}^{N-1} c_n \, \mathrm{e}^{-\mathrm{i}\delta_n t} \, |g_{2n-N+1}, \boldsymbol{p}+n\hbar(\boldsymbol{k}_+ - \boldsymbol{k}_-)\rangle , \quad (6)$$

where the weights c_n are related by

$$c_n = c_0 \left(\frac{-\Omega_+}{\Omega_-}\right)^n \frac{C_{-N+1}^{-N+2}\, C_{-N+3}^{-N+4} \cdots C_{2n-N-1}^{2n-N}}{C_{-N+3}^{-N+2}\, C_{-N+5}^{-N+4} \cdots C_{2n-N+1}^{2n-N}} , \quad (7)$$

and c_0 is chosen to normalize $|\varphi_{\mathrm{D}}\rangle$. Note that due to the recoil term quadratic in n the detunings δ_n cannot be tuned to zero simultaneously for $N > 2$ and $\boldsymbol{k}_+ \neq \boldsymbol{k}_-$. The dark state therefore is never completely stationary for a chain of Raman transitions, and "leaks" slightly [17]. In our experiment the duration of the optical pumping pulses is sufficiently short (of the order of a μs), so that the frequency width of the dark state [18] is larger than the recoil energy of four photons in frequency units (≈ 120 kHz).

We use here an open optical transition, such that if the laser fields are switched on the atoms within a closed momentum family are projected onto the dark state. All other atoms, after a few fluorescence cycles, are optically pumped into other hyperfine ground state levels that do not interact with the laser field any more. We neglect the small fraction of atoms that fall back into the dark state (of order $1/(2N-1)$ of the atoms falling back into the hyperfine state addressed by the laser field). In this approximation, a short optical projection pulse arriving at time t_{p} will convert an initial atomic wave function $|\Psi_{\mathrm{i}}(\boldsymbol{p})\rangle$ into a final wave function

$$\left|\Psi_{\mathrm{f}}(\boldsymbol{p}, t > t_{\mathrm{p}})\right\rangle = \left|\varphi_{\mathrm{D}}(\boldsymbol{p}, t_{\mathrm{p}})\right\rangle\left\langle\varphi_{\mathrm{D}}(\boldsymbol{p}, t_{\mathrm{p}})\right|\left.\Psi_{\mathrm{i}}(\boldsymbol{p})\right\rangle . \quad (8)$$

This formula is a special case of (11) in [15], where primarily the possibility of an adiabatic variation of the dark state by a slow change of the Rabi frequencies during a laser pulse was considered. We have assumed the pulse duration to be short compared to the inverse of all detunings δ_n.

1.2 Atom interferometers with dark states

Several papers have discussed the theory of atom interferometers based on optical $\pi/2$- and π-pulses [10, 19–21]. The theory of atom interferometer based on adiabatic transfer has been discussed in [9] and [15]. In the following, we describe the calculation of the atomic wave function obtained after a series of short optical projection pulses using a momentum basis picture [13, 14]. An atomic interferometer can be realized with a sequence of three projection pulses with equal times T between the first and second, and second and third optical pulse. For simplicity we assume that the Rabi-frequencies Ω_+ and Ω_- are equal.

1.2.1 Wave function approach. We first derive the interference signal for an initial plane atomic wave. The first pulse arriving at time t_{A} pumps the atoms into the dark state and

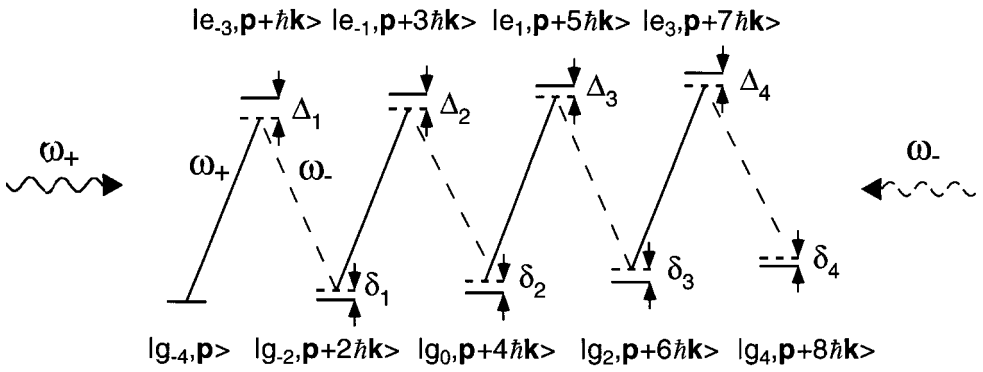

Fig. 2. Level scheme for a velocity dependent dark state including the kinetic energies of the components, and the detunings from resonance for two oppositely circularly polarized laser beams of frequencies ω_+ and ω_-

gives $|\Psi(\boldsymbol{p}, t_\mathrm{A})\rangle = |\varphi_\mathrm{D}(\boldsymbol{p}, t_\mathrm{A}^+)\rangle$. At the time $t = t_\mathrm{A} + T$ of the second pulse in general the atom is no longer completely dark for the light field. In the momentum basis picture used for our calculation this can be understood by the nonzero detuning factors δ_n, which make the dark state time dependent. With the second pulse, the wave function is projected onto the dark state that has evolved in time, and the resulting wave function is

$$
\begin{aligned}
&\left|\Psi(\boldsymbol{p}, (t_\mathrm{A}+T)^+)\right\rangle \\
&= |\varphi_\mathrm{D}(\boldsymbol{p}, t_\mathrm{A}+T)\rangle \ \langle\varphi_\mathrm{D}(\boldsymbol{p}, t_\mathrm{A}+T)|\varphi_\mathrm{D}(\boldsymbol{p}, t_\mathrm{A})\rangle \\
&= |\varphi_\mathrm{D}(\boldsymbol{p}, t_\mathrm{A}+T)\rangle \sum_{n=0}^{N-1} {c_n}^2 \ \exp\left[\,\mathrm{i}\,\delta_n T\,\right] \\
&= |\varphi_\mathrm{D}(\boldsymbol{p}, t_\mathrm{A}+T)\rangle \sum_{n=0}^{N-1} {c_n}^2 \\
&\quad \times \exp\left[\,\mathrm{i}\left(n(\Delta\omega - (\boldsymbol{k}_+ - \boldsymbol{k}_-)\,\boldsymbol{p}/m)\,T - n^2\omega_\mathrm{r} T\right)\right]. \qquad (9)
\end{aligned}
$$

This formula gives the interference signal for a multiple beam Ramsey experiment performed with two laser pulses and copropagating laser beams ($\boldsymbol{k}_+ = \boldsymbol{k}_-$, which gives also $\omega_\mathrm{r} = 0$). Such an experiment is described in [13] and is e.g. useful for measuring magnetic fields. We note that periodic rephasing of different magnetic sublevels was previously observed in the contrast of a two-beam atom interferometer, where the atoms in different sublevels formed independent interferometers [22]. One may apply the multiple beam Ramsey technique not only for measuring magnetic fields with increased resolution, but also in experiments testing for the permanent electric dipole moment (edm) of an atom [23] when applying a strong static electric field. Besides the higher resolution compared to experiments determining the difference frequency between two adjacent magnetic hyperfine levels, the multiple beam Ramsey technique can also have benefits in terms of systematic effects. The quadratic Stark effect, which shifts the magnetic sublevels by a value proportional to the square of the magnetic quantum number and is one of the major sources of systematic uncertainties in most edm experiments based on the former technique, here does not shift the fringe pattern since the experiment can be performed symmetrically in the magnetic sublevel quantum numbers m_F and $-m_F$ [1].

When using counterpropagating laser pulses unless one is really using a perfect monochromatic source of atoms, the fringe pattern at the second pulse will wash out, which in the momentum basis picture used in this calculation can be understood by the distribution of different Doppler shifts. Fringes can only be observed after a third laser pulse. We now assume that in the third pulse the phase of the light with frequency ω_+ is varied by an amount $\delta\theta$. This is equivalent to a change of the Raman detuning during the second pulse, so that $\Delta\omega$ is replaced by $\Delta\omega' = \Delta\omega + \delta\theta/T$ between the second and third pulse. The corresponding dark state is denoted as $|\varphi'_\mathrm{D}(\boldsymbol{p}, t)\rangle$. We obtain a wave function after the final pulse

$$
\begin{aligned}
&\left|\Psi(\boldsymbol{p}, (t_\mathrm{A}+2T)^+)\right\rangle \\
&= \left|\varphi'_\mathrm{D}(\boldsymbol{p}, t_\mathrm{A}+2T)\right\rangle \left\langle\varphi'_\mathrm{D}(\boldsymbol{p}, t_\mathrm{A}+2T)\middle|\varphi_\mathrm{D}(\boldsymbol{p}, t_\mathrm{A}+T)\right\rangle \\
&\quad \times \langle\varphi_\mathrm{D}(\boldsymbol{p}, t_\mathrm{A}+T)|\varphi_\mathrm{D}(\boldsymbol{p}, t_\mathrm{A})\rangle \\
&= \left|\varphi'_\mathrm{D}(\boldsymbol{p}, t_\mathrm{A}+2T)\right\rangle \sum_{n=0}^{N-1}\sum_{q=0}^{N-1} {c_n}^2 {c_q}^2 \\
&\quad \times \exp\left[\,\mathrm{i}\left((n+q)(\Delta\omega - (\boldsymbol{k}_+ - \boldsymbol{k}_-)\,\boldsymbol{p}/m)\,T\right.\right. \\
&\qquad \left.\left. + q\delta\theta - (n^2+q^2)\,\omega_\mathrm{r} T\right)\right]. \qquad (10)
\end{aligned}
$$

As stated above, in a real experiment there will be a distribution of different atomic momenta associated with the final size of the atomic wave packets, or also simply due to an inhomogeneous atomic velocity distribution. We can derive the expected interference signal from the plane wave solution of (10) by integrating over the atomic velocity distribution. Let us now assume counterpropagating optical beams with $\boldsymbol{k}_+ = k\boldsymbol{e}_z$ along the z-axis and $\boldsymbol{k}_- = -k\boldsymbol{e}_z$. The atomic velocity distribution along this axis will now introduce different Doppler shifts for the atoms. For simplicity we do not perform a momentum integration along the x- and y-axis.

Let us first derive the signal for an atomic wave packet with an initial momentum spread $f(p_z)$ along the z-axis. The wave function is derived from the plane wave solution of (10) using

$$
|\Psi_\mathrm{final}\rangle = \int \mathrm{d}\,p_z\ f(p_z)\ |\Psi(p_z, t_\mathrm{A}+2T)\rangle\ . \qquad (11)
$$

For the probability that an atom remains in the dark state after the final pulse one obtains

$$
\begin{aligned}
&|\,|\Psi_\mathrm{final}\rangle\,|^2 \\
&= \int \mathrm{d}\,p_z \int \mathrm{d}\,p'_z\ f(p_z)\ f^*(p'_z) \\
&\quad \times \left\langle\varphi'_\mathrm{D}(p'_z, t_\mathrm{A}+2T)\middle|\varphi'_\mathrm{D}(p_z, t_\mathrm{A}+2T)\right\rangle \\
&\quad \times \sum_{n=0}^{N-1}\sum_{q=0}^{N-1}\sum_{n'=0}^{N-1}\sum_{q'=0}^{N-1} {c_n}^2\, {c_q}^2\, {c_{n'}}^2\, {c_{q'}}^2 \\
&\quad \times \exp\left[\mathrm{i}\left((n+q-n'-q')(\Delta\omega - (2kp_z/m))\,T\right.\right. \\
&\qquad \left.\left. + (q-q')\delta\theta - (n^2+q^2-{n'}^2-{q'}^2)\,\omega_\mathrm{r} T\right)\right]. \qquad (12)
\end{aligned}
$$

This double integral reduces to a single integral by noting that the scalar product of the dark states equals zero unless p_z equals p'_z. The remaining single integral can be solved for an atomic velocity distribution sufficiently broad ($2k\Delta p_z T/m \gg 2\pi$) and smooth, such that the term $|\,f(p_z)\,|^2$ is approximately constant over a momentum interval of width $\delta p_z = \pi m/Tk$ and can be drawn before the integral. A sufficiently broad momentum width is intrinsically present for a wave packet well enough localized to allow a clear separation of the individual paths by the time of the second pulse. We only obtain a contribution different from zero when $n+q-n'-q' = 0$, and one sum sign can be omitted. We then obtain

$$
\begin{aligned}
|\,|\Psi_\mathrm{final}\rangle\,|^2 &= \sum_{n=0}^{N-1}\sum_{q=0}^{N-1}\sum_{q'=0}^{N-1} {c_n}^2\, {c_q}^2\, {c_{n+q-q'}}^2\, {c_{q'}}^2 \\
&\quad \times \exp\left[\mathrm{i}\left((q-q')(\delta\theta + (n-q')\,2\omega_\mathrm{r} T)\right)\right]. \qquad (13)
\end{aligned}
$$

[1] We note that, however, a loss of contrast can occur for larger times T, similarly as described below when discussing the effect of the recoil phase on the fringe pattern of the Doppler-sensitive atom interferometer. If the accumulated quadratic phase between adjacent even (or odd) magnetic sublevels reaches an integer multiple of 2π, one expects a revival of the fringe pattern.

Note that this result does not depend on $\Delta\omega$. Such an insensitivity to the frequency detuning is known for spin echo experiments. The result naturally is also independent of the centering, width and form of the atomic velocity distribution, provided only that the distribution does not vary significantly over a momentum interval δp_z as stated above. Using now a new index defined by $s = n + q$, the probability of finding an atom in the dark state after the pulses may be written as

$$|\,|\Psi_{\text{final}}\rangle\,|^2 = \sum_{s=0}^{2N-2} |\,|\Psi_s\rangle\,|^2\,, \tag{14}$$

where

$$|\Psi_s\rangle = \left(\sum_q c_{s-q}{}^2 c_q{}^2 \exp\left[\mathrm{i}\left(q\delta\theta + (sq-q^2)2\omega_r T\right)\right]\right) \times \left|\varphi_{D,s}\right\rangle\,. \tag{15}$$

As shown in Fig. 1 each wave function $|\Psi_s\rangle$ corresponds to $[N-(\,|\,s-N+1\,|\,)]$ beams that spatially recombine and interfere during the third pulse at position $[\boldsymbol{p}+s\hbar(\boldsymbol{k}_+ - \boldsymbol{k}_-)]\,T$ relative to the interferometer start. The $|\varphi_{D,s}\rangle$ denote the corresponding dark states at this time. The sum over the index q, which numbers the different possible paths in one family of interfering wave packets, runs from $\max(0,\ s-N+1)$ to $\min(N-1,\ s)$. The individual families give rise to different interference signals. Let us first consider the limit of small times T between the laser pulses ($\omega_r T \ll 1$), where the recoil term in (15) can be neglected. The contributions $|\,|\Psi_s\rangle\,|^2$ of the different families of interfering wave packets in this limit are shown in Fig. 3 for $N = 5$. Considering e.g. the family with two interfering beams ($s = 1$ and $s = 7$) one expects a sinusoidal interference signal. The sharpest principal maximum and three side maxima are obtained for the family with five interfering beams ($s = 4$), which also gives the largest contribution to the total signal. All these individual signals have their principal maxima at phases $\delta\theta$ of integer multiples of 2π. Note that these individual contributions do not precisely have the form of e.g. the far field diffraction pattern of a grating with several slits, since the different paths here do not all have equal weights. The unequal Clebsch–Gordan coefficients for the atom, analogous to e.g. a grating with different transmissions of the individual slits, will now increase the side maxima. For the case of an F to $F' = F$ transition as used here, one finds that the Clebsch–Gordan coefficients are such that the outermost paths are the ones mostly favored. The principal maximum of e.g. our five beam interference signal ($s = 4$ and $N = 5$) with a width of $0.16 \times 2\pi$ is therefore slightly sharper than the width obtained when setting all coefficients c_n to the same value (obtained width: $0.18 \times 2\pi$). While in principle by using a very well collimated atomic beam and performing spatially resolved detection one could observe the interference signals of the individual families ($s = 0,\ \ldots\ , 8$), in our experiment we measure the (incoherent) sum of all interference signals. The solid line in Fig. 3 shows the expected total interferometer signal, as given also by (14). Note that the plot gives the ratio of the number of atoms in the dark state after the third pulse to those in the dark state at the end of the first laser pulse. The signal observed in an experiment can be increased when adding a repumping laser during (at least part of) the first pulse, such that almost all the atoms can be prepared in the dark state.

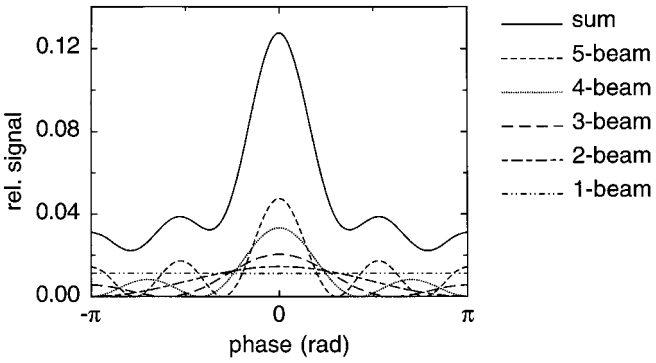

Fig. 3. Calculated individual signals of the families of interfering wave packets $|\,|\Psi_s\rangle\,|^2$ and total signal (*solid line*) of a multiple beam atom interferometer as shown in Fig. 1 with $N = 5$ paths for small times T between laser pulses ($\omega_r T \ll 1$, where $\omega_r = 2\hbar k^2/m$). The same signal is also obtained for $\omega_r T = r\pi$, where r is an integer number. The graph shows the fraction of atoms remaining in the dark state after the optical pulses as a function of the phase of the third pulse

Figure 4a shows theoretical total fringe signals for different drift times T between the laser pulses. For small times T, when the recoil term can be neglected, the phase difference between adjacent paths is equal for all paths. When for larger times T this term introduces phase shifts approaching unity between a central and an outermost path, the phase difference between adjacent paths within the interferometer is no longer constant for all paths. By variation of the phase $\delta\theta$ it is no longer possible to obtain constructive interference between all paths, and the width of the principal maxima decreases. The contrast of the interference pattern thus lessens for larger times T. When however the drift time T reaches an integer multiple of π/ω_r, the fringe pattern is revived. This can be seen from (15), since the recoil term now gives a phase equal to an integer multiple of 2π. Intuitively this effect is understood by considering the quadratic phase accumulated due to the photon recoil energy during a time $2T$ between the first and final optical pulse. When the accumulated phase difference between two adjacent paths approaches an integer multiple of 2π, the fringe pattern is revived. Collapse and revival of the fringe pattern are not observed in a two-beam atom interferometer[2]. These effects are interesting features of multiple beam interferometers. The recoil energy can be determined with a precise measurement of the revival time. In most other practical applications it will be reasonable to set the drift time T to a revival time, which maximizes the fringe contrast. Figure 4a further shows that at a drift time of half the first revival time (at $T = \pi/2\omega_r$) one also expects a fringe signal, which however shows a reduced contrast and doubled period. A fringe signal at $T = \pi/3\omega_r$ with tripled period is visible in Fig. 4a. When considering an atom interferometer with very many interfering paths, one generally expects fringes at $\omega_r T = r\pi/s$, with r and s as integer numbers.

[2]The incoherent sum of the signals of several two-beam atom interferometers with different phase terms can however in some cases also lead to a collapse and revival [22]. In a recent atom interferometer experiment based on three mechanical gratings, predominantly the signal of many two-beam atom interferometers of different geometries at revival times incoherently added up to an enhanced total signal [25].

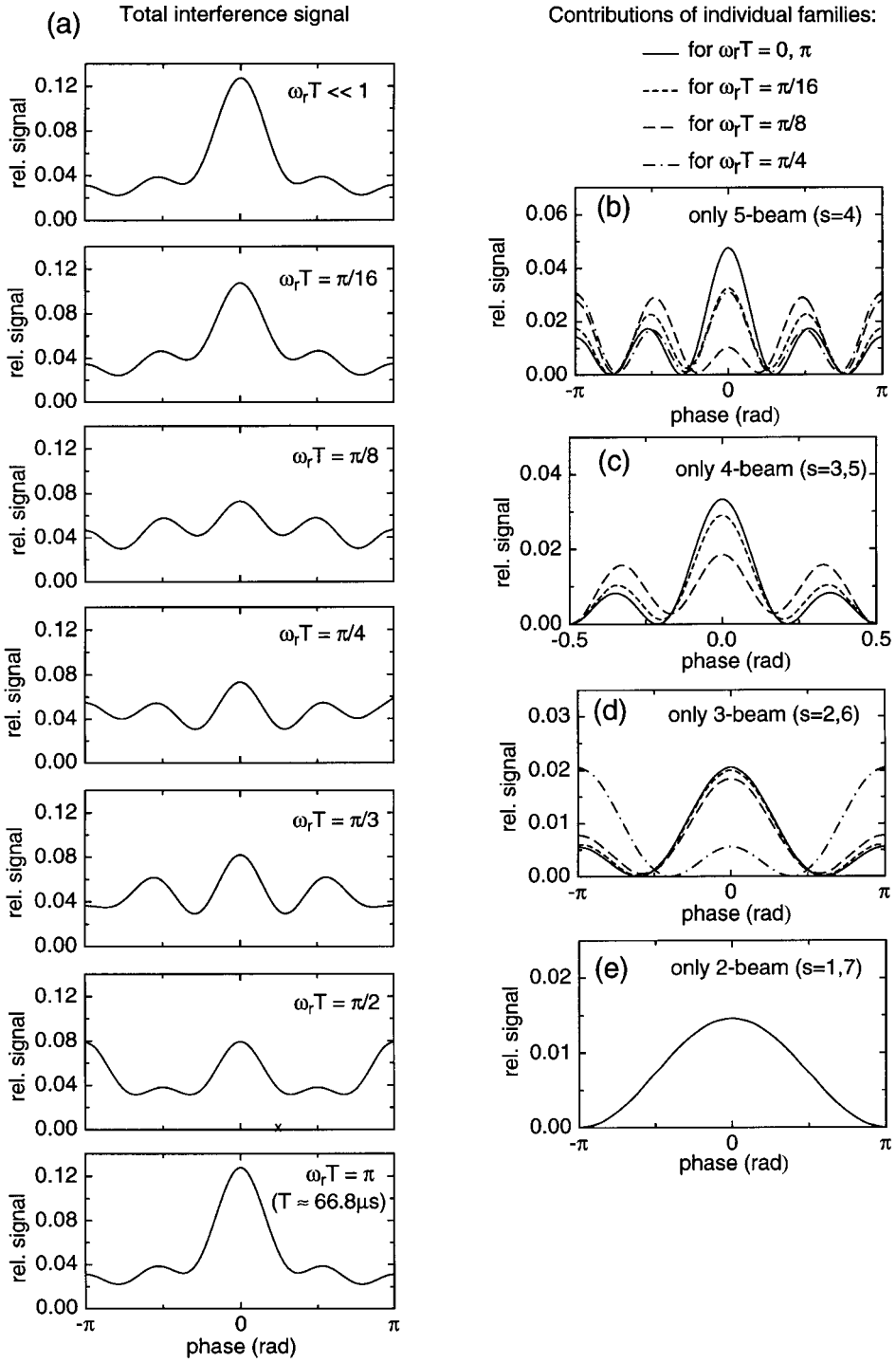

Fig. 4. a Calculated total interference signal of an atomic multiple beam interferometer with $N = 5$ paths for different drift times T between the laser pulses. While good interference contrast is expected for small times T, the signal soon collapses when T is increased. When the accumulated quadratic recoil phase between adjacent paths however equals an integer multiple of 2π for larger times T, a revival of the fringe signal occurs. **b – e** Signal of individual families of interfering wave packets, as shown in Fig. 1, for some different drift times T. The 4-beam signal for $\omega_r T = \pi/2$ in (**c**), and all 2-beam signals in (**e**) are equal to the corresponding signals at revival times. The 1-beam signal (s = 0 and 8) is independent of both the phase and T, and is not shown here

The signals of the individual families of interfering wave packets are shown in Figs. 4b–e for different times T between laser pulses. Similarly as for the total signal, collapse and revival is expected for the signals with more than two interfering wave packets. The interference signal with an increasingly large number of beams naturally degrade faster when departing from a revival time. Note that the signal of the individual families does not in all cases show period multiplying at drift times of integer fractions of the first revival time. For example, Figs. 4b–e shows that the signals of the families with an even number of interfering wave packets at a drift time of half the first revival time here are identical to the corresponding signal expected at a revival time, while the families with an odd number of wave packets at this intermediate time give a signal that is phase-shifted by π compared to the signal at revival time. We have, speaking very qualitatively, identified two mechanisms that can lead to period multiplying of the total interference signal. First, period multiplying of this sum signal can occur when the signals of individual families of interfering wave packets are phase-shifted by different amounts for some intermediate drift time. The period doubling of our five-beam signal at $\omega_r T = \pi/2$ shown in Fig. 4a

can be explained in this way, since this signal is an incoherent sum of families with principal maxima at phases of even and odd multiples of π for even respectively odd number of interfering wave packets. Second, the individual families can show period multiplying when the accumulated phase difference between paths differing by several photon momenta equals an integer number of integer multiple of 2π.

Collapse and revival effects related to the ones described are long known in near field optics, where it is not sufficient to solve the wave equation by keeping only terms linear in phase (Fraunhofer limit), but also including quadratic terms (Fresnel approximation). In this limit, e.g. self-imaging of periodic objects first observed by Talbot finds its explanation, as described e.g. in the review article by Patorski [24]. The Talbot effect has found first applications in atom optics and interferometry [1, 25–27], and also in the subrecoil cooling of atoms [28].

For future experiments, it certainly would be desirable to realize an atom interferometer with more than $N = 5$ paths. One might for example think of using some isotopes of heavy atoms or molecules with a high rotational quantum number and a very large number of m_F levels, which should result in interferometers with a very high number of interfering paths. The large enclosed area could increase the level of accuracy. Theoretical interference fringes for different number of paths N ($N = 2$, $N = 5$ and $N = 11$) are shown in Fig. 5 (left) as a function of the phase of the third pulse. Generally for such an interferometer with N paths both the width of the principal maxima and its height scale approximately as $1/N$ (for $N \gg 1$). Assuming Poissonian statistics the signal to noise ratio for a phase measurement therefore increases approximately as $\sqrt{N}$, when a repumping laser is added during the first laser pulse. The loss of signal that accompanies the fringe sharpening with more interfering paths occurs at the second laser pulse, which selects increasingly sharp velocity slices from the initial atomic velocity distribution. We note, that the same loss mechanism is also present in previously demonstrated interferometers based on adiabatic passage [9], and similarly also in the Bordé interferometer [10].

An increased number of interfering paths is also advantageous for a precise measurement of the revival time, from which the recoil energy can be readily determined (for a similar recoil energy measurement see also [27]). Figure 5 (right) gives the expected signal for multiple beam atom interferometers with different number of paths as a function of the drift time T between the pulses assuming no additional phase in the final pulse. A structure – caused by the recoil phase quadratic in transverse atomic momentum – is here only observed for more than two interfering paths ($N > 2$), which precisely is the condition for the occurance of collapse and revival when scanning the phase of the third pulse for different drift times T. Note that the expected fringe width for our method decreases with the square of the number of interfering paths[3], since multilevel coherences are excited. For a measurement of the photon recoil energy a $N^{3/2}$ scaling of the signal to noise ratio is thus obtained in the limit of Poissonian statistics.

1.2.2 Density matrix approach. We have furthermore verified that the results obtained in the previous section with a single particle wave function fully describe our experiments performed with an ensemble of atoms by calculating the interference signal in a density matrix approach. Again we only consider the atomic momentum along the z-axis of the laser beams. For the sake of simplicity we further assume that the spatial extend of the atomic beam along this axis is infinite, and thus in a momentum basis picture no diagonal elements between different momentum states occur. A more general initial atomic density matrix for an atomic beam can be found in [31].

The first laser pulse performed at time t_A projects the atoms onto a dark state, and the resulting density matrix by this time is

$$\varrho(t_\mathrm{A}) = \int \mathrm{d}\, p_\mathrm{z}\, g(p_\mathrm{z})\ |\varphi_\mathrm{D}(p_\mathrm{z}, t_\mathrm{A})\rangle\, \langle\varphi_\mathrm{D}(p_\mathrm{z}, t_\mathrm{A})|\ , \tag{16}$$

where $g(p_\mathrm{z})$ here includes both the quantum mechanical momentum spread of an atomic wave packet, and the classical atomic velocity distribution of an ensemble of atoms with different initial velocities. The density matrix obtained after three optical projection pulses can readily be determined from (10), and gives

$$\begin{aligned}\varrho_\mathrm{final} &= \int \mathrm{d}\, p_\mathrm{z}\, g(p_\mathrm{z})\ \ |\Psi(p_\mathrm{z}, t_\mathrm{A}+2T)\rangle\, \langle\Psi(p_\mathrm{z}, t_\mathrm{A}+2T)| \\ &= \int \mathrm{d}\, p_\mathrm{z}\, g(p_\mathrm{z})\ \ \left|\varphi'_\mathrm{D}(p_\mathrm{z}, t_\mathrm{A}+2T)\right\rangle\left\langle\varphi'_\mathrm{D}(p_\mathrm{z}, t_\mathrm{A}+2T)\right| \\ &\quad \times \sum_{n=0}^{N-1}\sum_{q=0}^{N-1}\sum_{n'=0}^{N-1}\sum_{q'=0}^{N-1} {c_n}^2\, {c_q}^2\, {c_{n'}}^2\, {c_{q'}}^2 \\ &\quad \times \exp\left[\mathrm{i}\left((n+q-n'-q')\,(\Delta\omega - (2kp_\mathrm{z}/m))\,T\right.\right. \\ &\quad \left.\left. + (q-q')\delta\theta - (n^2+q^2-{n'}^2-{q'}^2)\,\omega_\mathrm{r}T\right)\right]. \end{aligned} \tag{17}$$

If the momentum of the atoms in the dark state is not resolved, we can omit the quantum number p_z in the dark states and draw the obtained states $|\varphi'_\mathrm{D}(t_\mathrm{A}+2T)\rangle\langle\varphi'_\mathrm{D}(t_\mathrm{A}+2T)|$ out of the integral. Similarly to the procedure described in the discussion of (12), we can solve the momentum integral for an atomic velocity distribution sufficiently broad ($2k\Delta p_\mathrm{z}T/m \gg 2\pi$) and smooth. In the resulting expression we again use the index $s = n+q$, and our final result can be written in the simple form

$$\varrho_\mathrm{final} = \sum_{s=0}^{2N-2} |\Psi_s\rangle\, \langle\Psi_s|\ , \tag{18}$$

where $|\Psi_s\rangle$ is given by (15) and describes the wave function of a single family of interfering paths. Note that this density matrix does not include the atoms lost during the projection pulses, most of which will be optically pumped into an other hyperfine level and not detected. With the density matrix approach, we obtain the same fringe pattern as derived previously using wave functions only.

[3] In the well known Bordé-Interferometer [10] with four optical pulses, where the propagation direction of the light pulses is reversed after the second pulse, the photon recoil can be determined also with two interfering beams from the frequency splitting between the central fringes of two different interferometers. Also in that scheme an increased recoil can be obtained, when using multipulse sequences to transfer additional photon momenta to the atoms within the atom interferometer. The observed recoil splitting increases linearly [29], or even with the square of the number of transferred photon momenta [30].

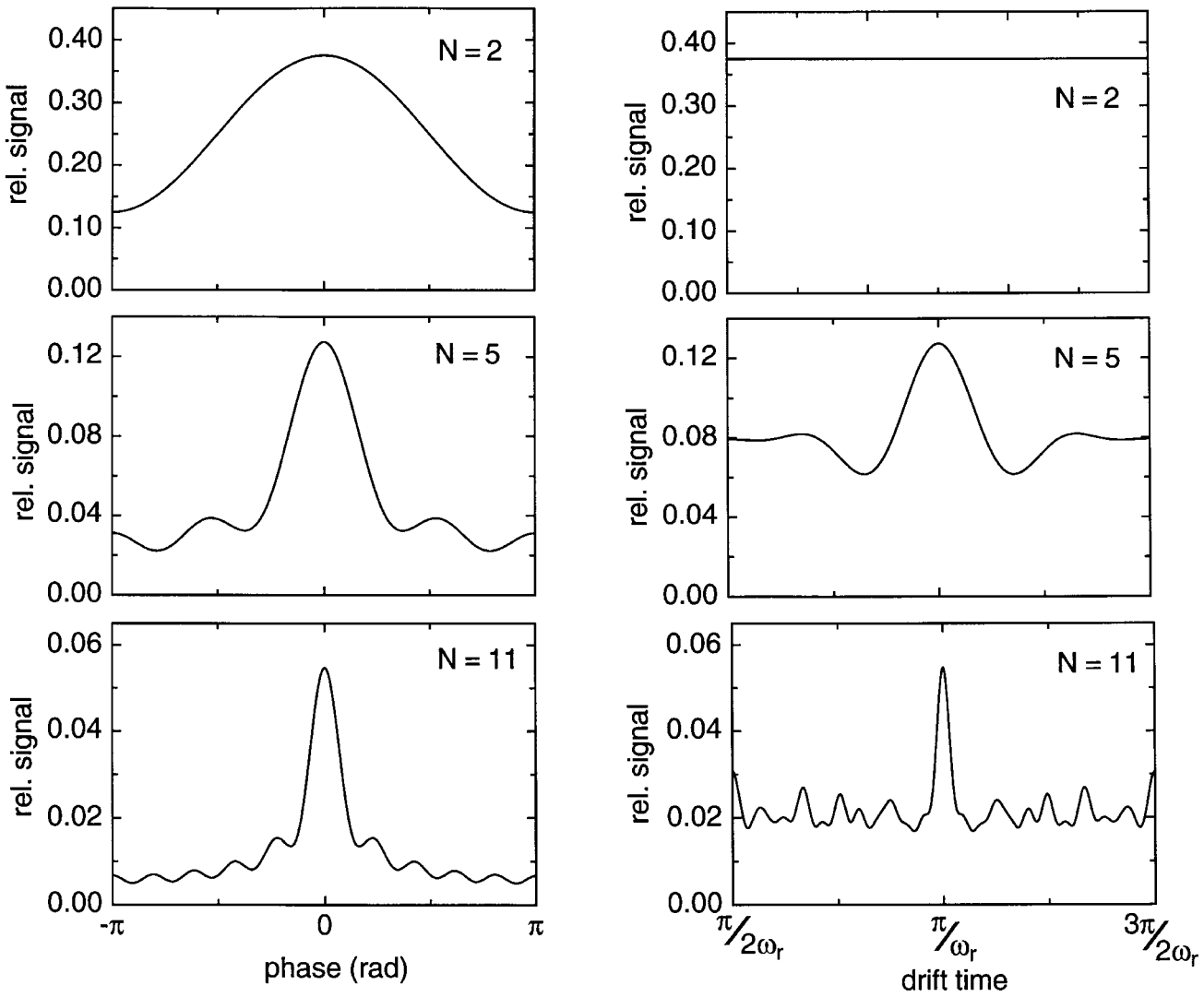

Fig. 5. Calculated total interference signals for multiple beam atom interferometer with different number of interfering paths N, as can be realized using an atom with a transition from a ground state of total angular momentum $F = N-1$ to an excited state with $F' = F$: (*left*) as a function of the phase of the third optical pulse at a revival time ($T = \mathrm{r}\pi/\omega_\mathrm{r}$, with r as an integer number), and (*right*) as a function of the drift time T between the optical pulses with no additional phase of the third pulse

1.3 The atomic coherence length

Let us, in a density matrix approach, now derive the signal expected after only two laser pulses, if the phase of the second laser pulse is varied. The density matrix of atoms in the dark state by this time is

$$\begin{aligned}\varrho'(t_\mathrm{A}+T) = {} & \left|\varphi'_\mathrm{D}(t_\mathrm{A}+T)\right\rangle\left\langle\varphi'_\mathrm{D}(t_\mathrm{A}+T)\right| \\ & \times \int \mathrm{d}\,p_\mathrm{z}\, g(p_\mathrm{z}) \sum_{n=0}^{N-1}\sum_{n'=0}^{N-1} {c_n}^2\, {c_{n'}}^2 \exp\left[\mathrm{i}\,(n-n')\right. \\ & \left. \times \left((\Delta\omega - (2kp_\mathrm{z}/m))\, T + \delta\theta - (n+n')\,\omega_\mathrm{r} T \right)\right].\end{aligned} \tag{19}$$

When the atomic velocity distribution is sufficiently broad and smooth ($2k\Delta p_\mathrm{z} T/m \gg 2\pi$) such that $g(p_\mathrm{z})$ does not vary significantly over an interval $\delta p_\mathrm{z} = \pi m/Tk$, the term $g(p_\mathrm{z})$ can again be replaced by a constant and drawn before the integral. The signal after the second pulse is determined by the density matrix

$$\varrho'(t_\mathrm{A}+T) = \left|\varphi'_\mathrm{D}(t_\mathrm{A}+T)\right\rangle\left\langle\varphi'_\mathrm{D}(t_\mathrm{A}+T)\right| \sum_{n=0}^{N-1} {c_n}^4, \tag{20}$$

which is independent of the phase $\delta\theta$, and the fringes at this point average out. The condition for a sufficiently broad velocity distribution to cause a washing out of the fringes at the second pulse is equivalent to the condition that the splitting between adjacent interferometer paths $2T\hbar k/m$ is much larger than the spatial coherence length of the atoms $z_\mathrm{coh} = \hbar/2\Delta p_\mathrm{z}$. The (transverse) spatial coherence length equals the minimum size of an atomic wave packet with momentum width Δp_z. Earlier work originated by neutron interferometer experiments has shown, that while the size of a wave packet increases with time due to diffraction, the spatial coherence length of a wave packet remains constant over time [32]. In our experiments, the splitting between adjacent paths exceeds the coherence length, and no fringes are observed with only

two pulses when using counterpropagating optical beams. A fringe signal can only be observed with a sequence of three laser pulses that spatially divide, redirect, and then recombine the atomic wave packets. By experimentally verifying that the spatial splitting between adjacent paths by the time of the second pulse exceeds the atomic coherence length, one justifies the assumption of a sufficiently broad atomic velocity distribution to derive (14) and (18) from the plane wave signal of (10).

1.4 Inertial measurements

We now derive the sensitivity of the atom interferometer to some inertial fields. Assume that the atoms are subject to a gravitational field with acceleration $\boldsymbol{g}$, and that the setup is rotated with a constant angular velocity $\boldsymbol{\Omega}$. We follow [33], and consider the variation of the laser frequencies due to the inertial fields in the frame of an atom with initial velocity $\boldsymbol{v}$. The resulting modification of the interferometer signal is derived by modifying the frequency detunings from resonance accordingly in (4) and (5). The fringe signal changes only due to the variation in the Raman laser difference detunings δ_n, where the term: $\omega_+ - \omega_-$ is replaced by: $\omega_+ - \omega_- - (\boldsymbol{k}_+ - \boldsymbol{k}_-)\cdot\boldsymbol{g}\,t - (\boldsymbol{k}_+ - \boldsymbol{k}_-)\cdot\boldsymbol{\Omega}\times\boldsymbol{v}\,t$. The corresponding interferometer signal is obtained by replacing the phase $\delta\theta$ with the term: $\delta\theta - (\boldsymbol{k}_+ - \boldsymbol{k}_-)\cdot\boldsymbol{g}\,T^2 - (\boldsymbol{k}_+ - \boldsymbol{k}_-)\cdot\boldsymbol{\Omega}\times\boldsymbol{v}\,T^2$ in (15). The fringe pattern is shifted uniformly, and by this the degree of rotation or acceleration can be determined. As discussed in Sect. 1.2, compared to the corresponding two-beam atom interferometer a higher resolution can be obtained here due to the narrower fringe width.

2 Experimental Setup

Our experimental setup is schematically shown in Fig. 6. Within a vacuum chamber, cesium atoms are emitted by an oven trough a 200 μm wide slit into an atomic beam. The beam is collimated in a direction along the optical pumping beams by a second slit of 250 μm width in a distance of 25 cm. The atoms then enter an optical interaction region, which is magnetically shielded and has a homogeneous (typically 9 mG) magnetic bias field oriented along the optical beams. Within the interaction region the cesium atoms are irradiated by a series of three optical light pulses. The pulses are generated from a Ti:sapphire laser near 894 nm. After passing a first acousto-optic modulator (AOM) used to generate the pulse shapes for the optical beams, the light is split to provide the two counter-propagating optical projection beams in a σ^+–σ^- polarization configuration. Each of the beams then passes a further AOM which shifts their optical frequencies by slightly different amounts in order to maintain the two-photon resonance condition ($\Delta\omega = 0$) in the presence of the bias field. The phase of the rf drive frequency of one of these frequency shifters can be changed during the pulse sequence to allow the adjustment of the phase of one of the optical beams in the final pulse. The two projection beams are spatially filtered and expanded to Gaussian beam diameters of 43 mm. The typical optical power in each beam is 300 mW. All the interferometer pulses are applied during the transit time of the atoms through the optical interaction region. While in earlier experiments using a slightly simplified setup still without magnetic shielding we have observed the fringe pattern by detecting the atomic fluorescence emitted in the final optical selection pulse [13], in later experiments we have measured the number of atoms remaining in the dark state (in $F = 4$) after the pulses. This population is measured by irradating the atoms with a further optical detection pulse tuned to the $6S_{1/2}\,(F = 4) - 6P_{3/2}\,(F' = 5)$ cycling transition, and recording the resulting fluorescence with a photomultiplier and a boxcar integrator. The optical detection beam is generated with a diode laser, and is travelling in opposite direction of the atomic beam to allow Doppler selection of only a part of the broad thermal atomic velocity distribution. The frequency of the diode laser is tuned to address atoms moving with a velocity near 140 m/s, while the most probable velocity of the beam is 290 m/s. This Doppler selection efficiently suppresses signal contributions from atoms moving far above the most probable atomic velocity, so that a significant increase of the interferometer drift time is obtained.

In a typical pulse sequence, we start the first interferometer pulse with a 1.2 μs long period of lower light intensity to select a velocity slice Δv_z of $2k\Delta v_z/2\pi \approx 200$ kHz Doppler width in the direction along the optical pumping beams from the initial transverse beam velocity distribution of 1.2 MHz Doppler width (we refer here to the width for a Raman-like two-photon transition). The beam power is then increased to full value for the remaining time of the 2 μs long pulse. The typical length of the second and third interferometer pulse is 1.2 μs. Subsequently, the population in the dark state is measured. The repetition rate of such an interferometer pulse sequence is 3.5 kHz. We alternate between a sequence with

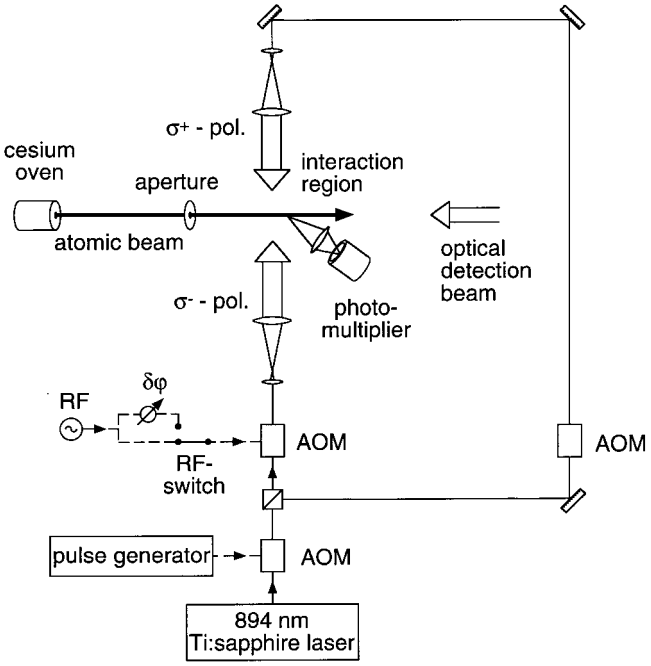

Fig. 6. Experimental setup of the multiple beam atom interferometer. The atoms in the atomic beam are irradiated by a sequence of three laser pulses with two counterpropagating optical beams and σ^+ respectively σ^- circular polarization. In the third pulse, the RF-switch is flipped such that the phase of the drive frequency of the acoustooptic modulator is shifted by an amount $\delta\theta$. The atomic interference signal can be monitored either by observation of the fluorescence emitted during the third optical pulse, or by recording the fluorescence scattered from a further optical detection beam

the phase of the beam with frequency ω_+ shifted in the final pulse, and a sequence with no additional phase shift. We determine the difference of the two obtained fluorescence signals with a lock-in amplifier, which largely suppresses the effect of stray light. The typical used integration time is 1 s per measurement point.

3 Experimental results

The solid line in Fig. 7 shows a typical interferometer signal obtained by measuring the fluorescence scattered during the third optical pumping pulse, where the atomic wave function is recombined in several families of interfering wave packets. This spectrum was recorded for a time $T = 5\,\mu$s between sucessive light pulses, where $\omega_r T \ll 1$. Note that the fluorescence signal here decreases in the interference maxima, since little fluorescence is emitted in the final pulse when the atoms by this time are dark for the light field. The observed width of the principal dip typically is $0.32 \times 2\pi$ which is clearly broader than the expected value of $0.18 \times 2\pi$. As discussed below, we believe that this larger width of the interferometer signal is both due to the broad transverse atomic velocity distribution and to imperfect optical wavefronts. The observed width nevertheless is still considerably below the value $0.5 \times 2\pi$ observed in conventional two-beam interferometer experiments. Related multiple beam atom interferometer experiments have now also been realized by two other groups [27, 34]. The dashed line in Fig. 7 for comparison shows the signal measured during the second pulse as a function of the phase of this pulse. In this case almost no interference signal is observed, which is an indication that by this time the spatial splitting between two adjacent paths exceeds the atomic coherence length. The spatial splitting between adjacent paths after a drift time T is $2T\hbar k/m = T \cdot (6.67\,\text{mm/s})$, while the atomic coherence length corresponding to the atomic velocity width selected during the first laser pulse is $z_{\text{coh}} = \hbar/2m\Delta v_z \approx 2.7\,\text{nm}$.

In later experiments, as stated above, we have improved our experimental setup to allow longer drift times between the interferometer pulses. We have added an additional laser tuned to the $6S_{1/2}\,(F=4) - 6P_{3/2}\,(F'=5)$ cycling transition, which was pulsed on directly after the third selection pulse to allow measurement of the number of atoms left in the dark state (in $F = 4$) by the scattered fluorescence. In this way, we have recorded interference signals such as those shown in Fig. 8 as a function of the phase of the third projection pulse for different times T between the laser pulses. The lowest curve with $T = 5\,\mu$s corresponds to the atomic interference signal in the limit of small times between laser pulses ($\omega_r T \ll 1$), as in the spectrum shown in Fig. 7. Note however, that the signal of atoms in the dark state shown in Fig. 8 increases in the interference maxima, as in the theoretical fringe patterns of Figs. 3–5. While good contrast of the interference pattern is observed in Fig. 8 for small times T between the laser pulses, the fringe pattern collapses for drift times T above a few μs. This collapse of the fringe pattern is expected for multiple beam atom interferometers, and is caused by a recoil phase shift, that inreases quadratically in transverse atomic momentum. When the drift time reaches $T = \pi/2\omega_r$ (equals approximately 33.4 μs), one expects a partial regain of constrast and a period doubling, which is only barely visible. When the drift time however approaches the first revival time at $T = \pi/\omega_r$ (approximately 66.8 μs), the fringe pattern is restored, and the fringes reach maximum contrast at the revival time. For this time, the accumulated quadratic phase between adjacent paths has reached an integer multiple of 2π. For even larger drift times between the pulses, the fringe pattern again collapses. These results directly demonstate the temporal Talbot effect in an atom interferometer. The observation of collapse and revival is both fundamentally interesting and of practical importance, since it shows that multiple beam atom interferometers can be realized with longer drift times between laser pulses, as necessary for precision measurements.

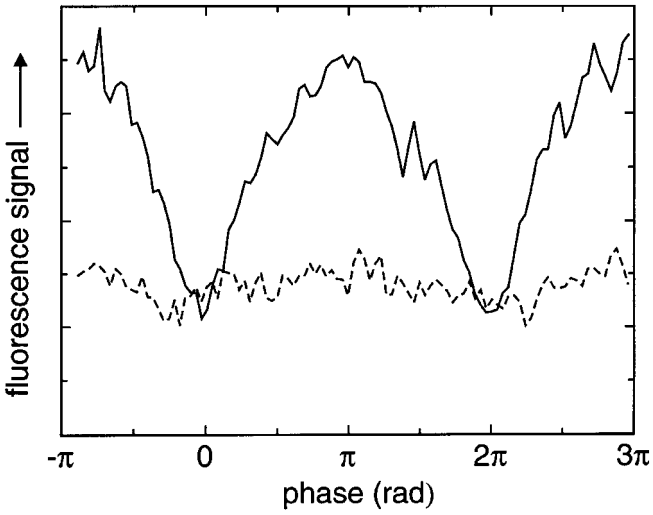

Fig. 7. Experimental interference signals (*solid*) of an atomic multiple beam interferometer realized with a sequence of three optical pulses, as shown in Fig. 1 for a time $T = 5\,\mu$s between laser pulses. The fluorescence signal detected during the third pulse is shown as a function of the phase of this pulse. Note that this signal decreases in the interference maxima. For comparison, the dashed line shows the fluorescence detected during the second pulse as a function of the phase of the second pulse. Since the splitting between the individual paths by this time exceeds the spatial coherence length, almost no interference signal is present

The typically observed fringe width of the principal maxima increases from $0.32 \times 2\pi$ at small drift times to $0.36 \times 2\pi$ at the first revival time, both of which is above the theoretical value, but below the fringe width of two-beam atom interferometers. With the aim of determining the cause of the experimental fringe broadening, we have observed Doppler-free multilevel Ramsey interference signals [13] by orienting the two Raman beams in a colinear excitation geometry. The typical observed Ramsey fringe width in our new setup with magnetic shielding was $0.20 \times 2\pi$ for a drift time of 130 μs, which is reasonably near to the expected value of $0.16 \times 2\pi$. One thus does not expect inhomogeneous stray magnetic fields to be the principle cause for the broadening of the atom interferometer fringes. We attibute the broadening of these spectra, recorded in the Doppler-sensitive mode with counterpropagating laser beams, to be mainly due to both the large initial atomic velocity spread parallel to the laser beams and to imperfect optical wavefronts. Wavefront imperfections are expected to be important especially for larger drift times, since then each atom samples light from different spatial regions within the optical beams. Note that the fringe pattern of Fig. 8 is shifted slightly towards higher phases for larger drift

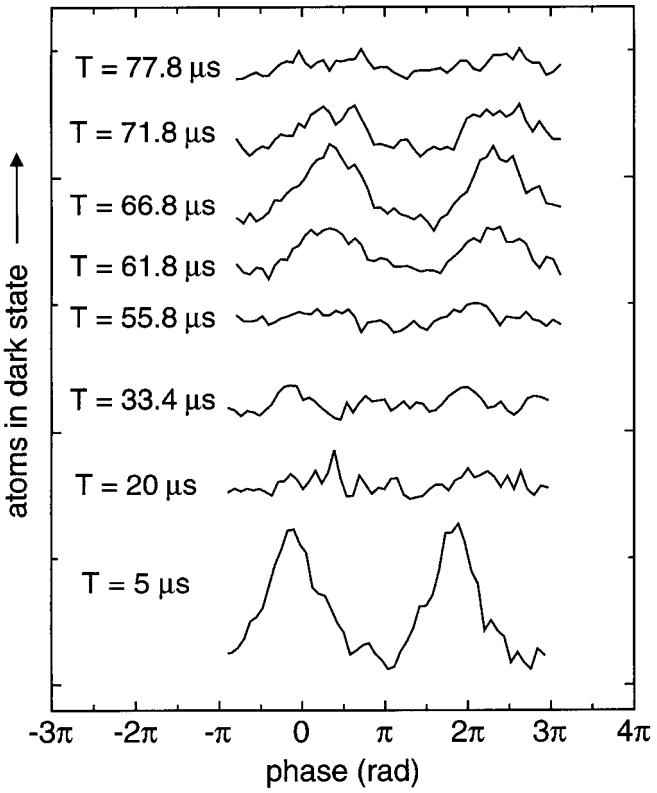

Fig. 8. Experimental interference signals for different drift times T between the laser pulses. This plot shows the number of atoms detected after the projection pulses as a function of the phase of the third pulse. The signal here increases in the interference maxima. For drift times T above several µs the signal collapses. When the time T approaches the first revival time of π/ω_r (equals about 66.8 µs for the cesium D1 line) the fringe pattern revives. For even larger times T the fringe contrast again decreases. We note that the data with T above 50 µs had to be taken with a higher photomultiplier supply voltage

times, which also may be due to wavefront imperfections. The magnitude of this shift changed between experimental runs only after a major realignment of the optical interferometer beams. As can be seen from (15), a principal interference maximum is expected at zero phase independent from (homogeneous) magnetic field or frequency detuning. The multilevel Ramsey signal is less affected by imperfect optics, since for Doppler-free signals both beams are copropagating and can pass through the same optics.

We have monitored the optical beam quality with an optical sheering interferometer, and estimate an average, mainly spherical symmetric phase distortion of almost half a fringe between the center and the edge of the 60 mm diameter beams. For comparsion, during the total interferometer drift time $2T$ the atoms with velocity 140 m/s typically travel a distance of approximately 20 mm across the laser beam at the first revival time. Moreover, the atoms are located at different positions within the beam profile when being irradiated by the optical pulses. We attribute the beam imperfections to be mainly due to unexpectedly large spherical aberations of our collimation doublet lenses (N. A. $1/30$), and to imperfections of the vacuum can windows. We expect good optical beam quality to be especially important for multiple beam atom interferometers, since multiphoton coherences are required. Besides choosing very high quality optics, in a future experimental setup based on slow atoms the interferometer beams could be oriented colinearly to the propagation direction of the atoms. Beam quality imperfections are then expected to affect the interference signal less even at very large drift times, since the atoms in their free flight then mostly sample light that passed though the same spatial region of the optical components [9, 29].

4 Outlook

In future experiments, drift times up to 200 ms and narrower fringe width should be within reach by using laser cooled cesium atoms in an atomic fountain [35]. Precision measurements of, e.g. gravitation and photon recoil should be possible with an increased sensitivity. One might also think of using dark states with components differing only in their external, and not in their internal quantum numbers. Since then one would no longer be limited by the number of internal levels, a larger number of interfering paths might be realized[4]. The difficulty in such a scheme is, that the dark state then would tend to extend to both positive and negative very large momenta, and thus is extremely leaky for finite pulse lengths due to the quadratic recoil phase. A multiple beam atom interferometer based on this scheme could be realized by using a sequence of three resonant standing waves tuned to an open optical transition [36]. In a simplified spatial picture, only those atoms are dark that pass precisely through the nodes of the waves. An atom interferometer realized with three resonant standing waves tuned to an open optical transition in the short pulse limit does in many terms resemble an atom interferometer realized with an arrangement of three mechanical gratings [25, 37]. In contrast to these experiments, however, by using optical absortion gratings losses at the first grating could in principle be much reduced when a repumping laser is added during the first laser pulse.

To conclude, atom interferometers with dark states are intriguing applications of quantum mechanics. In the future, they will allow for more precise measurements of both fundamental and applied interest.

[4] When performing the calculation of the fringe pattern of such an atom interferometer one finds a mathematically equivalent result to the fringe pattern derived in this work [see e.g. (14)], where however the weights c_n of the dark state with, in theory, infinitely many components will not reach a stationary value within an optical pumping pulse of finite length, and thus are always dependent on length and intensity of a pulse. A second important difference to the calculation presented in Sect. 1.2 is, that one here can extend the integral over the atomic velocity distribution along the direction of the laser beams (11) only over a momentum range of $2\hbar k$ to avoid double counting of the components of the dark state. It follows, that one can derive the far field solution of (13) only when the drift time T equals at least the first revival time at $T = \pi/\omega_r$, since the momentum interval δp_z is naturally limited to $2\hbar k$. The far field interference pattern of (14) is thus only observed for a drift time of at least the first revival time (more precisely, the period doubling, tripling etc. effects described by (14) can already be observed at times $T = \pi/(s\omega_r)$ with s being an integer number). For smaller times, one has to consider the full solution of (12), which also describes near field (geometrical shadow) effects.

References

1. See, for example, articles in *Atom Interferometry*, ed. by P. Berman (Academic Press, San Diego 1997)
2. L. Marton, J.A. Simpson, J.A. Suddeth: Phys. Rev. **90**, 490 (1954); G. Möllenstedt: Naturwiss. **42**, 41 (1955)
3. H. Maier-Leibnitz, T. Springer: Z. Phys. **167**, 386 (1962); H. Rauch, W. Treimer, U. Bonse: Phys. Lett. A **57**, 369 (1972)
4. See, for example: E. Hecht, A. Zajac: *Optics* (Addison-Wesley, Reading 1974)
5. A. Aspect, E. Arimondo, R. Kaiser, N. Vansteenkiste, C. Cohen-Tannoudji: Phys. Rev. Lett. **61**, 826 (1988)
6. P. Marte, P. Zoller, J.L. Hall: Phys. Rev. A **44**, R4118 (1991)
7. J. Lawall, M. Prentiss: Phys. Rev. Lett. **72**, 993 (1994)
8. L.C. Goldner, C. Gerz, R.J.C. Spreeuw, S.L. Rolston, C.I. Westbrook, W.D. Phillips, P. Marte, P. Zoller: Phys. Rev. Lett. **72**, 997 (1994)
9. M. Weitz, B.C. Young, S. Chu: Phys. Rev. Lett. **73**, 2563 (1994)
10. C.J. Bordé: Phys. Lett. A **140**, 10 (1989)
11. M. Kasevich, S. Chu: Phys. Rev. Lett. **67**, 181 (1991)
12. E.L. Hahn: Phys. Rev. **80**, 580 (1950)
13. M. Weitz, T. Heupel, T.W. Hänsch: Phys. Rev. Lett. **77**, 2356 (1996); M. Weitz, T. Heupel, T.W. Hänsch: Verh. DPG (VI) **31**, 258 (1996)
14. M. Weitz, T. Heupel, T.W. Hänsch: Europhys. Lett. **37**, 517 (1997); M. Weitz, T. Heupel, T.W. Hänsch: Verh. DPG (VI) **32**, 347 (1997)
15. M. Weitz, B.C. Young, S. Chu: Phys. Rev. A **50**, 2438 (1994)
16. G. Alzetta, A. Gozzini, L. Moi, G. Orriols: Nuovo Cimento B **36**, 5 (1976); E. Arimondo, G. Orriols: Lett. Nuovo Cimento **1**7, 333 (1976); H.R. Gray, R.M. Whitley, R. Stroud, Jr.: Opt. Lett. **3**, 218 (1978)
17. C.J. Foot, H. Wu, E. Arimondo, G. Morigi: J. Phys. II **4**, 1913 (1994), and references therein.
18. C. Cohen-Tannoudji: In *Les Houches 1990, Session LIII*, ed. by J. Dalibard, J.-M. Raimond, J. Zinn-Justin (North-Holland, Amsterdam 1992).
19. C.J. Bordé, C. Salomon, S. Avrillier, A. Van Lerberghe, C. Bréant, D. Bassi, G. Scoles: Phys. Rev. A **30**, 1836 (1984)
20. R. Friedberg, S.R. Hartmann: Phys. Rev. A **48**, 1446 (1993)
21. P. Storey, C. Cohen-Tannoudji: J. Phys. II **4**, 1999 (1994)
22. J. Schmiedmayer, C.R. Ekstrom, M.S. Chapman, T.D. Hammond, D.E. Pritchard: J. Phys. II **4**, 2029 (1994)
23. See, for example: N.F. Ramsey: In *Atomic Physics 14*, ed. by D.J. Wineland, C.E. Wieman, S.J. Smith (AIP, New York 1995)
24. K. Patorski: *Progress in Optics XXVII*, ed by. E. Wolf (North-Holland, Amsterdam 1989)
25. J.F. Clauser, S. Li: Phys. Rev. A **49**, R2213 (1994)
26. M.S. Chapman, C.R. Ekstrom, T.D. Hammond, J. Schmiedmayer, B. Tannian, S. Wehinger, D.E. Pritchard: Phys. Rev. A **51**, R14 (1995)
27. S.B. Cahn, A. Kumarakrishnan, U. Shim, T. Sleator, P.R. Berman, B. Dubetsky: submitted to Phys. Rev. Lett.
28. F. Sander, T. Devolder, T. Esslinger, T.W. Hänsch: Phys. Rev. Lett. **78**, 4023 (1997); see also the contribution by T. Esslinger, F. Sander, T.W. Hänsch in this volume.
29. D.S. Weiss, B.C. Young, S. Chu: Phys. Rev. Lett. **70**, 2706 (1993)
30. C.J. Bordé, M. Weitz, T.W. Hänsch: In *Laser Spectroscopy XI*, ed. by L. Bloomfield, T. Gallagher, D. Larson (AIP, New York 1994)
31. B.-G. Englert, C. Miniatura, J. Baudon: J. Phys. II **4**, 2043 (1994)
32. H. Kaiser, S.A. Werner, E.A. George: Phys. Rev. Lett. **50**, 560 (1983); A.G. Klein, G.I. Opat, W.A. Hamilton: Phys. Rev. Lett. **50**, 563 (1983); see also the discussion by U. Sterr, K. Sengstock, W. Ertmer, F. Riehle, J. Helmcke in [1]
33. M. Kasevich, S. Chu: Appl. Phys. B **54**, 321 (1992)
34. A. Pautz, H. Rieger, J.L. Peng, F. Ruschewitz, K. Sengstock, W. Ertmer: Verh. DPG (VI) **32**, 348 (1997)
35. M. Kasevich, E. Riis, S. Chu, R.G. DeVoe: Phys. Rev. Lett. **63**, 612 (1989)
36. We note that a two-beam atom interferometer using also an open optical transition has been demonstated with variable finite laser detuning: E.M. Rasel, M.K. Oberthaler, H. Batelaan, J. Schmiedmayer, A. Zeilinger: Phys. Rev. Lett. **75**, 2633 (1995)
37. D.W. Keith, C.R. Ekstrom, Q.A. Turchette, D.E. Pritchard: Phys. Rev. Lett. **66**, 2693 (1991)